Appl. Phys. A 88, 377–383 (2007)
DOI: 10.1007/s00339-007-3989-6
Applied Physics A
Materials Science & Processing

K. PRASAD[1,✉]
LILY[1]
K. KUMARI[1]
K.P. CHANDRA[2]
K.L. YADAV[3]
S. SEN[4]

Electrical properties of a lead-free perovskite ceramic: $(Na_{0.5}Sb_{0.5})TiO_3$

[1] Materials Research Laboratory, University Department of Physics, T.M. Bhagalpur University, Bhagalpur 812007, India
[2] Department of Physics, S.M. College (T.M. Bhagalpur University), Bhagalpur 812001, India
[3] Department of Physics, Indian Institute of Technology, Roorkee 247667, India
[4] National Metallurgical Laboratory, Jamshedpur 831007, India

Received: 16 November 2006 / Accepted: 16 February 2007
Published online: 26 April 2007 •

ABSTRACT Polycrystalline $(Na_{0.5}Sb_{0.5})TiO_3$ was prepared using a high-temperature solid-state reaction method. An XRD analysis indicated the formation of a single-phase monoclinic structure. Complex impedance studies revealed the presence of grain boundary effects from 300 °C onwards. Also, the dielectric relaxation in the system was found to be of a non-Debye type. The ac conductivity data were used to evaluate the density of states at the Fermi level, the minimum hopping length and activation energy of the compound. The dc electrical and thermal conductivities of grain and grain boundary have been assessed. The correlated barrier hopping model was found to successfully explain the mechanism of charge transport in $(Na_{0.5}Sb_{0.5})TiO_3$.

PACS 72.20.Ee; 77.22.Ch; 77.22.Gm; 77.84.Dy; 81.05.Je

1 Introduction

Lead-bearing compounds, $PbTiO_3$, $Pb(Zr, Ti)O_3$, $Pb(Mg_{1/3}Nb_{2/3})O_3$, are widely used for capacitor, pyroelectric and piezoelectric applications. Recently, European legislation on waste electrical/electronic equipment has been issued. The use of hazardous substances such as lead in electrical parts is prohibited from 2006 [1]. To meet this requirement the search for alternative environment friendly lead-free materials, for these applications have become the focal theme of current research. In recent years a number of perovskite ABO_3-type lead-free materials have been studied for the potential application [1–15]. Sodium bismuth titanate, $(Na_{0.5}Bi_{0.5})TiO_3$ (NBT) is considered to be an excellent candidate as a key material for lead-free piezoelectric ceramic, which shows strong ferroelectric properties [10, 11, 16–20]. NBT belongs to the perovskite family (ABO_3-type) with rhombohedral symmetry at ambient temperature. The recent work on the identical compounds $(Na_{0.5}La_{0.5})TiO_3$ [14] and $(Na_{0.5}Bi_{0.5})ZrO_3$ [15] showed excellent electrical properties. One such ceramic in this series is perovskite $(Na_{0.5}Sb_{0.5})TiO_3$ (NST). The material is mechanically tough and lead-free.

Residual conductivity in the bulk of the grains of such systems has been found to be around 10^{-7} S m^{-1} in the operating temperature region [15]. The high insulating property is mainly due to the fact that grain boundaries in the dielectric material act as high resistive barriers for the cross transport of charge carriers. Therefore proper understanding of the effect of grain boundaries for evaluating overall behaviour of the ceramic samples is important. Complex impedance spectroscopy (CIS) has been recognized as a non-destructive powerful technique to study the microstructure and the electrical properties of solids [21]. Thus, the dynamics of ionic movement and contributions of various microstructure elements such as grain, grain boundary and interface polarization to total electric response in polycrystalline solids can be identified by this technique. It also enables us to evaluate the nature of dielectric relaxation and the relaxation frequency of the material.

An extensive literature survey indicated that no attempt, to the author's knowledge, has so far been made to study $(Na_{0.5}Sb_{0.5})TiO_3$. The present work is an attempt to study the role of grain and grain boundaries on the electrical behaviour of NST and their dependence on temperature and frequency using complex impedance spectroscopy technique. The structural, microstructural, dielectric, impedance and ac conductivity studies on NST ceramic have been presented. Also, an attempt has been made to explain the conduction mechanism in the system.

2 Experimental

$(Na_{0.5}Sb_{0.5})TiO_3$ was obtained from AR grade (99.9%+ pure) chemicals (Na_2CO_3, Sb_2O_3 and TiO_2) by a solid-state synthesis route in accordance with the following thermo-chemical reaction at 1100 °C for 4 h:

$$0.25\,Na_2CO_3 + 0.25\,Sb_2O_3 + TiO_2 \xrightarrow{\Delta} (Na_{0.5}Sb_{0.5})TiO_3\,. \quad (1)$$

A circular disc shaped pellet having a thickness = 0.97 mm and diameter = 10.11 mm was made by applying an uniaxial stress of 6 MPa. The pellet was subsequently heated at 1150 °C under oxygen for 3 h. Completion of the reaction and the formation of the desired compound were checked by X-ray diffraction techniques. The XRD spectra were taken on calcined powders of NST with an X-ray diffractometer (Siemens D500) at room temperature, using Co K_α radiation ($\lambda = 1.7902$ Å), over a wide range of Bragg angles

✉ Fax: +91 641 2501699, E-mail: k_prasad65@yahoo.co.in

($20° \leq 2\theta \leq 80°$) with a scanning speed of 2° min^{-1}. The microstructure of the sintered NST sample was taken on the fractured surface using a computer controlled scanning electron microscope (JEOL-JSM840A). The electrical measurements were carried out on a symmetrical cell of type Ag|NST|Ag, where Ag is a conductive paint coated on either side of the pellet. Electrical impedance (Z), phase angle (θ), loss tangent ($\tan\delta$) and capacitance (C) were measured as a function of frequency (0.1 kHz–1 MHz) at different temperatures (40–500 °C) using a computer-controlled LCR Hi-Tester (HIOKI 3532-50), Japan. The ac conductivity data was obtained from impedance data, using a relation $\sigma_{ac} = t/(AZ')$ where Z' is the real part of impedance, t and A are the thickness and area of the sample, respectively.

3 Results and discussion

3.1 *Structural and microstructural studies*

Figure 1 shows the XRD-profile of NST at room temperature. A standard computer program (POWD) was utilized for the XRD-profile analysis. Good agreement between the observed and calculated inter-planer spacing and no trace of any extra peaks due to constituent oxides, were found, thereby suggesting the formation of a single-phase compound having a monoclinic structure. The lattice parameters were found to be: $a = 4.077(5)$ Å, $b = 9.233(0)$ Å, $c = 6.524(1)$ Å and $\beta = 91.266°$ with an estimated error of $\pm 10^{-3}$ Å. The unit cell volume was estimated to be 245.56 $Å^3$. The average crystallite size of NST was estimated from some strong reflections of low 2θ values of XRD profile using Scherrer's equation:

$$P_{hkl} = 0.89\lambda/\beta_{1/2}\cos\theta\,, \tag{2}$$

where $\beta_{1/2}$ = peak width of the reflection at half height and was found to be about 7 nm. The criterion adopted for evaluating the rightness, reliability of indexing and the structure of compound was the sum of differences in observed and calculated d-values [i.e. $\sum \Delta d = \sum(d_{obs} - d_{calc})$] which were minimized using least square refinement technique. Inset Fig. 1 illustrates the enlarged version of the representative (100) peak. A Gaussian model was applied to analyse the curve.

$$I = I_o + (A/w\sqrt{\pi/2})\exp[-2\{(\theta-\theta_c)/w\}^2]\,, \tag{3}$$

where A, w and θ_c are respectively the area, width and center of the curve. The fitting parameters as obtained for NST are

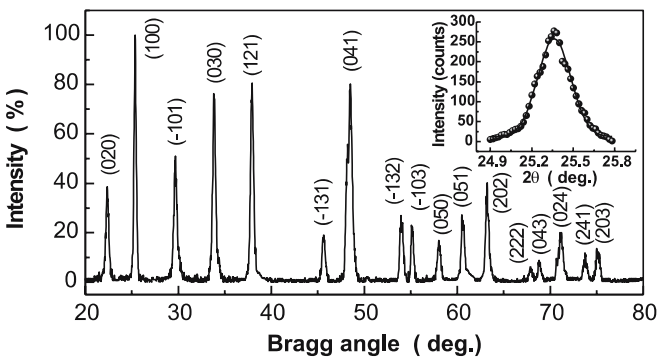

FIGURE 1 Indexed X-ray diffraction pattern of NST at room temperature. *Inset*: enlarged view of the (100) peak with a Gaussian fit

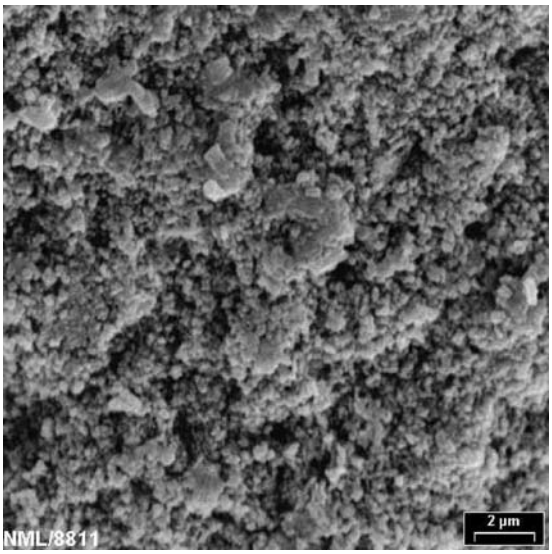

FIGURE 2 SEM micrograph of $(Na_{0.5}Sb_{0.5})TiO_3$ at 2 μm magnification

$I_o = 12.1131$, $A = 73.4467$, $w = 0.239$ and $\theta_c = 25.3612$. The value of regression coefficient (R^2) was found to be 0.9895.

Figure 2 shows the SEM-micrograph of NST at 2 μm magnification. Grain shapes are clearly visible, indicating the existence of a polycrystalline microstructure. The grain of unequal sizes appears to be distributed throughout the sample. The average grain size was estimated to be about 0.5 μm. The ratio of average crystallite size to the grain size of NST is found to be of the order of 10^{-2}.

3.2 *Dielectric study*

Figure 3 shows the frequency dependence of the real (ε') and imaginary parts (ε'') of the dielectric constant

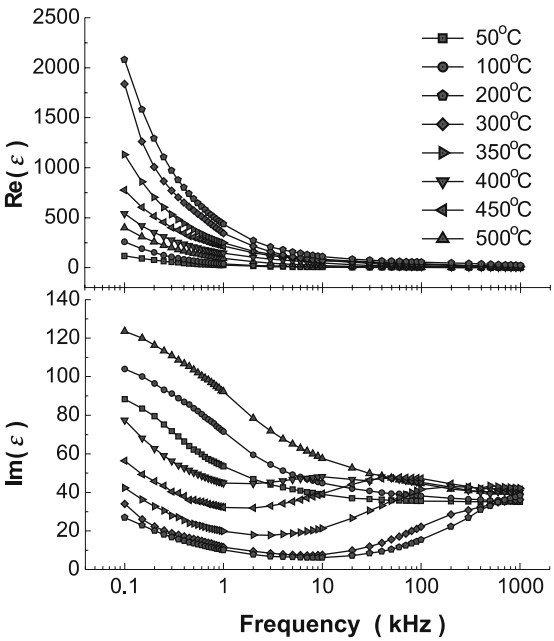

FIGURE 3 Frequency dependence of the real and imaginary parts of the dielectric constant for NST at different temperatures

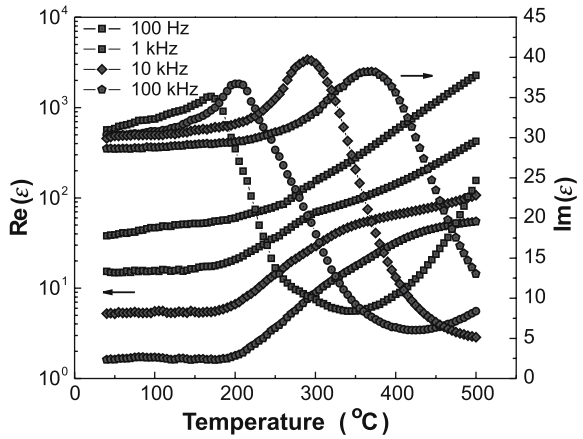

FIGURE 4 Temperature dependence of the real and imaginary parts of the dielectric constant for NST at different frequencies

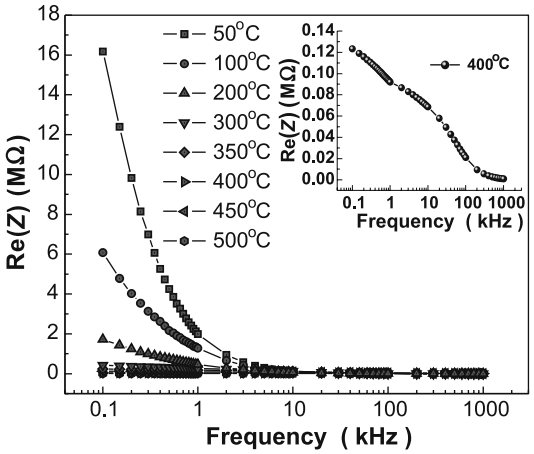

FIGURE 5 Variation of real part of impedance of NST with frequency at different temperatures. *Inset* shows the representative plot at 400 °C

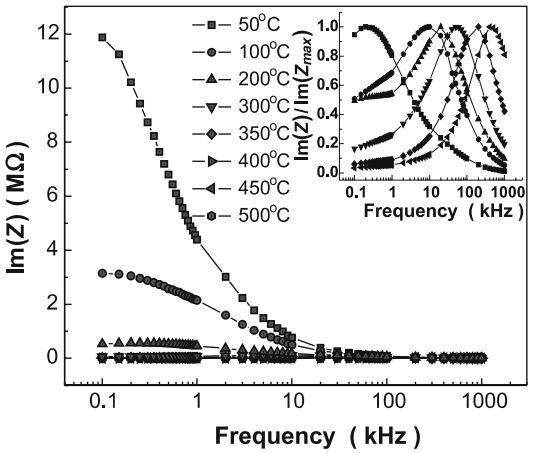

FIGURE 6 Variation of the imaginary part of impedance of NST with frequency at different temperatures. *Inset* shows the scaled imaginary part of impedance with frequency at different temperatures

at several temperatures. It is observed that ε' follows an inverse dependence on frequency, normally followed by almost all dielectric/ferroelectric materials. Also, the value of ε'' decreases with an increase in frequency in the low temperature region, while at higher temperatures, it finds a minimum which shifts to the high frequency side. Furthermore, the pattern presents the dispersion in the lower frequency region. The Debye formula giving the complex permittivity, related to the free dipole oscillating in an alternating field, is given by:

$$\varepsilon^* = \varepsilon' - \mathrm{i}\varepsilon'' = \varepsilon_\infty + \frac{\varepsilon_s - \varepsilon_\infty}{1 + \mathrm{i}\omega\tau}\,. \tag{4}$$

The real part of ε is given by

$$\varepsilon' = \varepsilon_\infty + \frac{\varepsilon_s - \varepsilon_\infty}{1 + (\omega\tau)^2}\,, \tag{5}$$

where ε_s and ε_∞ are the low and high frequency values of ε', $\omega = 2\pi f$, f being the frequency of measurement and τ the relaxation time. A relatively high dielectric constant at low frequencies is a characteristic of a dielectric material. At very low frequencies ($\omega \ll 1/\tau$), dipoles follow the field and we have $\varepsilon \approx \varepsilon_s$ (value of dielectric constant at quasi static fields). As the frequency increases (with $\omega < 1/\tau$), dipoles begin to lag behind the field and ε' slightly decreases. When the frequency reaches the characteristic frequency ($\omega = 1/\tau$), the dielectric constant drops (relaxation process) and at very high frequencies ($\omega \gg 1/\tau$), dipoles can no longer follow the field and thereby $\varepsilon' \approx \varepsilon_\infty$. Qualitatively, the same behaviour is observed in the material studied in the present work as shown in Fig. 3. Figure 4 presents the thermal response of ε' and ε'' at different frequencies for NST. It is observed that the value of ε' increases while ε'' finds a maxima which shifts to the higher temperature side with the increase of frequency in the investigated temperature range.

3.3 *Impedance study*

Figure 5 shows the variation of the real part of impedance (Z') with frequency at various temperatures. It is observed that the magnitude of Z' decreases on increasing temperature, and the frequency shows a negative temperature coefficient of resistance (NTCR) type behavior of the NST, indicating an increase in ac conductivity with the rise in temperature and frequency. A representative curve (inset Fig. 5) indicates that the system has a grain boundary contribution also. The loss spectrum (Fig. 6) is characterized by some important features in the pattern, such as the appearance of a peak ($Z''_{\max}$), asymmetric peak broadening (inset Fig. 6). The values of $Z''_{\max}$ decrease which shift to higher temperatures with increasing frequency. The asymmetric broadening of peaks in the frequency plots of Z'' suggests that there is a spread of relaxation times i.e. the existence of a temperature dependent electrical relaxation phenomenon in the material [21]. Inset Fig. 6 shows the normalized imaginary parts $Z''/Z''_{\max}$ of the impedance as a function of frequency for NST at several temperatures. It seems that high temperature (≥ 300 °C) triggers another (grain boundary) relaxation process.

Figure 7 shows the complex impedance plots at different temperatures. It is observed that these curves do not coincide with the origin and hence there is a series resistance R_s that can be ascribed to the LCR circuit representation (inset Fig. 6) of the sample [22]. It can be seen from Fig. 8 that the value

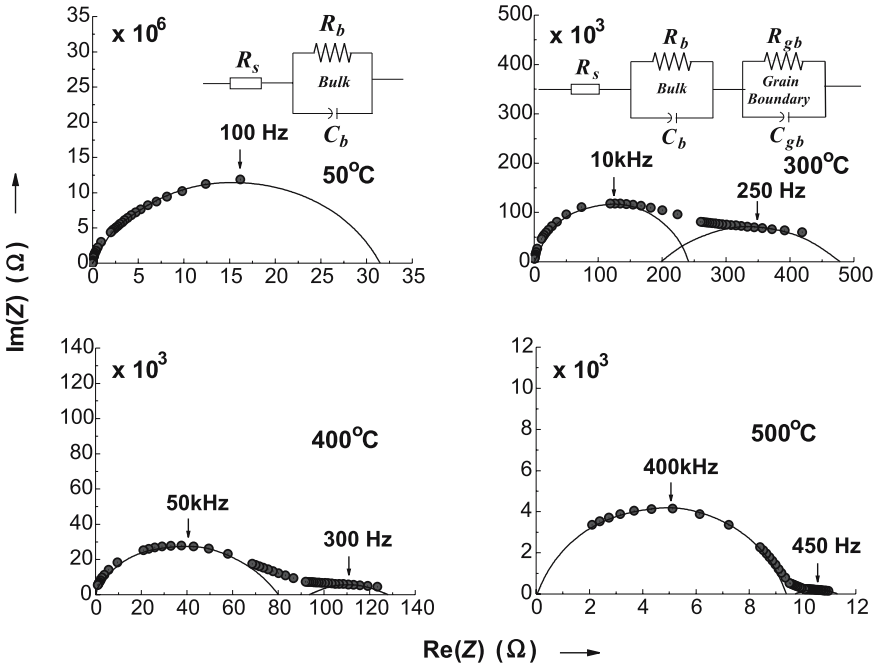

FIGURE 7 Complex impedance plots of NST at different temperatures. *Inset* shows the appropriate equivalent electrical circuit

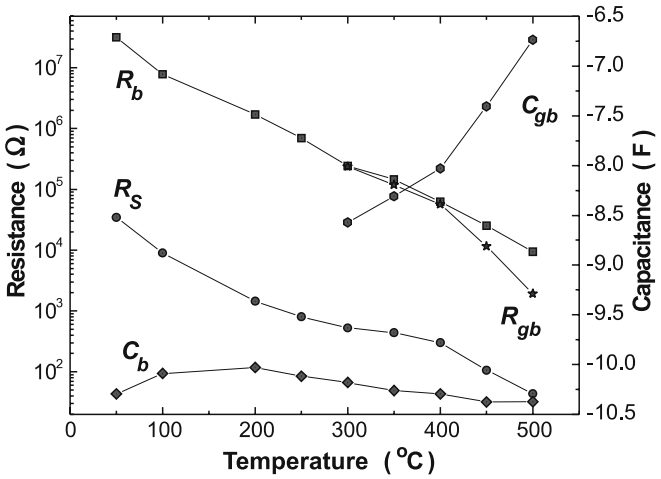

FIGURE 8 Variation of R_s, R_b, R_{gb}, C_b and C_{gb} with the temperature of NST

of R_s decreases with increasing temperature. For a semicircle at 50 °C and from 300 °C onwards, two semicircles could be obtained with different values of resistance for grain (R_b) and grain boundary (R_{gb}). Hence, grain and grain boundary effects could be separated at these temperatures. It can also be observed that the peak maxima of the plots decrease and the frequency for the maximum shifts to higher values with the increase in temperature. The dielectric relaxation in the system can be assessed through complex impedance plots. For Debye type relaxation, the center of the semicircle should be located on the Z'-axis, whereas for non-Debye type relaxation these argand plane plots are close to semicircular arcs with end-points on the real axis, and the center should lie below this axis. The complex impedance in such situations can be described as:

$$Z^*(\omega) = Z' + \mathrm{i}Z'' = R/[1 + (\mathrm{i}\omega/\omega_o)^{1-\alpha}]\,, \qquad (6)$$

where α represents the magnitude of the departure of the electrical response from an ideal condition and this can be determined from the location of the center of the semicircles, when $\alpha \to 0$, (6) gives rise to classical Debye's formalism. It can be seen that the complex impedance plots are not represented by a full semicircle, rather center that the semicircular arc lies below the Z'-axis ($\alpha > 0$) suggesting the dielectric relaxation to be of a non-Debye type. This may be due to the presence of distributed elements in the material–electrode system [22]. Also, it is found that the value of α increases with the rise in temperature. The correlation among the Debye relaxators may start developing via formation of nanopolar clusters of Na–TiO_3 and Sb–TiO_3 [15, 23]. Since the relaxation times of the relaxators within polar clusters are distributed over a wide spectrum at higher temperatures, their response to external fields are in a different time domain. This results in the deviation from Cole–Cole plots. It is clear from Fig. 7 that with the increase of measuring temperature Cole–Cole plots split into two discrete semicircles, inferring the possible average profile of various Cole–Cole semicircles. The split semicircles may be due to secondary elements like interfacial capacitance or defects. The first semicircle (may be ascribed to a parallel combination of bulk resistance, R_b and capacitance, C_b) in the high frequency region, corresponds to the behaviour of intragranular of the material or bulk properties. The second semicircle (may be attributed to a parallel combination of grain boundary resistance, R_{gb} and capacitance, C_{gb}), in the low frequency region, and represents the grain boundary contribution. It is known that the conductivities of grains and grain boundaries may be different owing to the different underlying processes, and thereby they relax in different frequency regions. In such cases the equivalent circuits (inset Fig. 7) can be represented as a series network of parallel RC elements [22]. Impedance can then be represented as:

$$Z^* = (R_b^{-1} + j\omega C_b)^{-1} + (R_{gb}^{-1} + j\omega C_{gb})^{-1}\,, \qquad (7)$$

where

$$Z' = R_b/\left[1+(\omega R_b C_b)^2\right] + R_{gb}/\left[1+(\omega R_{gb} C_{gb})^2\right], \quad (8)$$

and

$$Z'' = \omega R_b^2 C_b/\left[1+(\omega R_b C_b)^2\right] + \omega R_{gb}^2 C_{gb}/\left[1+(\omega R_{gb} C_{gb})^2\right]. \quad (9)$$

The values of R_b and R_{gb} could directly be obtained from the intercept of the ends of the semicircle on the Z'- axis whose variation with temperature is shown in Fig. 8. It can be seen that the value of R_b and R_{gb} decrease with the rise of temperature, which clearly indicates the NTCR character of NST and supports Fig. 5. The capacitances (C_b and C_{gb}) due to these effects can be estimated using the relation:

$$\omega_{max} RC = 1, \quad (10)$$

where $\omega_{max} (= 2\pi f_{max})$ is the angular frequency at the maximum of the semicircle. Figure 8 shows the temperature variation of C_b and C_{gb} obtained from Cole–Cole plots at different temperatures. The decrease in the value of R_b of NST associated with an increase in conductivity with the rise in temperature. Also, a decrease in R_{gb} values with the increment in temperature suggests the lowering of the barrier to the mobility of charge carriers aiding electrical conduction at higher temperatures.

3.4 *Electrical conductivity study*

The ac electrical conductivity, in most of the materials due to localized states is given by the relation:

$$\sigma_{ac} = \sigma(0) + \sigma(\omega), \quad (11)$$

where $\sigma(\omega)$ and $\sigma(0)$ are respectively, the frequency dependent and independent part of the conductivity. Figure 9 shows the log–log plot of electrical conductivity versus frequency at different temperatures. The pattern of the conductivity spectrum shows dispersion throughout the chosen frequency range. The frequency dependence of ac conductivity obeys the relation of type [24]:

$$\sigma_{ac} = A_1 \omega^{S_1} + A_2 \omega^{S_2}, \quad (12)$$

where A_1 and A_2 are the temperature dependent constants and s_1 and s_2 are temperature as well as frequency dependent parameters. Such dependence is associated with the displacement of carriers which move within the sample by discrete hops of length R between randomly distributed localized sites. The values of the indexes s_1 and s_2 can respectively, be obtained from the slopes of the plots $\log \sigma_{ac}$ vs. $\log \omega$ in the low and high frequency regions. The inset of Fig. 9 shows the temperature dependence of s_1 and s_2. It can be seen that the values of both s_1 and s_2 are always less than 1 and decrease with the rise of temperature. Further, the value of $s_1 \to 0$ at higher temperatures indicates that dc conductivity dominates at higher temperatures in the low frequency region and following (11). The model based on correlated hopping of electrons over the barrier [25] predicts a decrease in the value of the index with the increase in temperature, and so is found to be

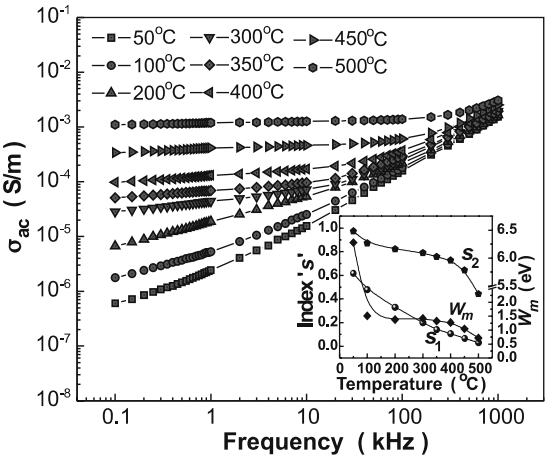

FIGURE 9 Variation of ac conductivity with frequency at different temperatures for NST. *Inset* shows the variation of exponents s_1, s_2 and binding energy with temperature

consistent with the experimental results. Therefore, the electrical conduction in the system could be considered as due to the short-range translational type hopping of charge carriers [24–26]. This indicates that the conduction process is a thermally activated process. The exponent s_i ($i = 1$ or 2) and binding energy is related as:

$$s_i = 1 - (6k_B T/W_m). \quad (13)$$

A decreasing trend of W_m with temperature has been observed (inset Fig. 9). The characteristic decrease in slopes (s_1 and s_2) with the rise in temperature is due to the decrease in binding energy.

The ac conductivity data have been used to evaluate the density of states at Fermi level $N(E_f)$ using the relation [27]:

$$\sigma_{ac}(\omega) = (\pi/3) e^2 \omega k_B T \{N(E_f)\}^2 \alpha^{-5} \{\ln(f_o/\omega)\}^4, \quad (14)$$

where e is the electronic charge, f_o the photon frequency and α is the localized wave function, assuming $f_o = 10^{13}$ Hz, $\alpha = 10^{10}\ m^{-1}$ at various operating frequencies and temperatures. Figure 10 shows the frequency dependence of $N(E_f)$ at different temperatures. It can be seen that the plots show a minimum up to 300 °C. After this temperature the minimum starts disappearing and the value of $N(E_f)$ decreases with the increasing frequency. Further, it can be noticed the minima shift towards higher frequency side and the value of $N(E_f)$ increases with the rise in temperature. The reasonably high values of $N(E_f)$ suggest that the hopping between the pairs of sites dominate the mechanism of charge transport in NST [15].

The hopping conduction mechanism is generally consistent with the existence of a high density of states in the materials having a band gap like that of a semiconductor. Due to localization of charge carriers, formation of polarons takes place and the hopping conduction may occur between the nearest neighboring sites. Figure 11 shows the variation of bulk/grain and grain boundary conductivities, obtained from the impedance data (Fig. 7) against $10^3/T$. The nature of variation obeys the Arrhenius relationship:

$$\sigma = \sigma_o \exp(-E_a/k_B T), \quad (15)$$

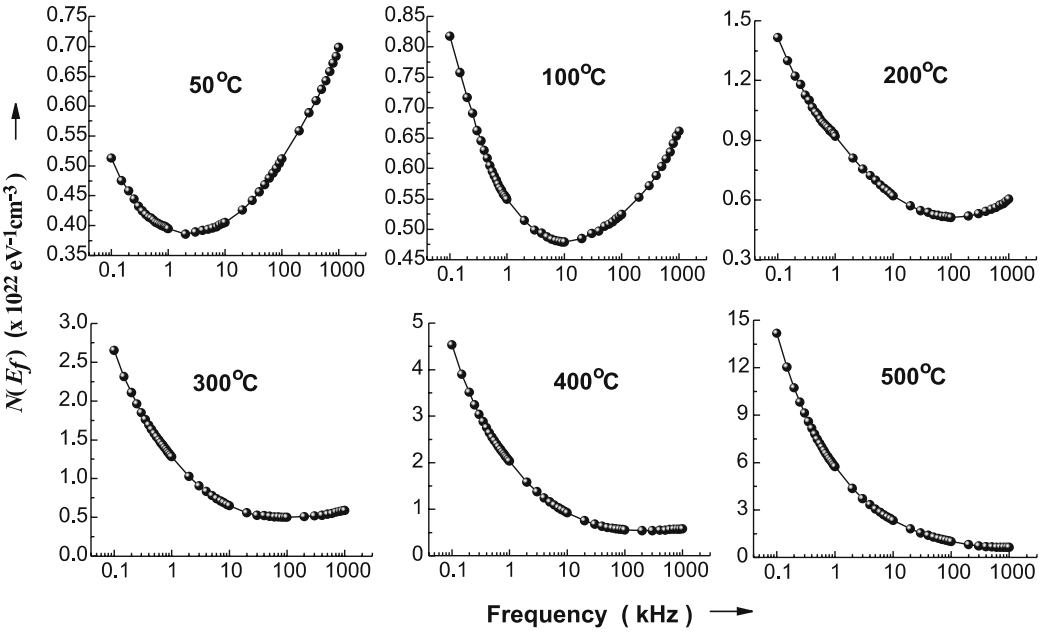

FIGURE 10 Frequency dependence of $N(E_f)$ of NST at different temperatures

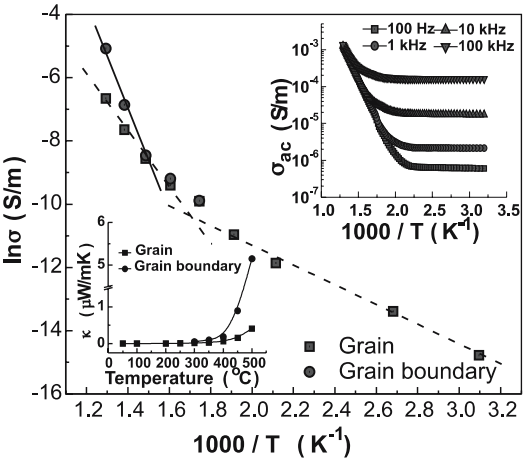

FIGURE 11 Variation of grain and grain boundary conductivity of with the inverse of temperature for NST. *Inset 1* shows the temperature dependence of ac conductivity at different frequencies. *Inset 2* shows the variation of thermal conductivity of grain and grain boundarys with temperature

where E_a is the activation energy of conduction and T is the absolute temperature. The nature of variation shows the negative temperature coefficient of resistance (NTCR) behaviour of NST. The linear least squares fitting to the conductivity-temperature data given the values of E_a for grain and grain boundary. A variation of the slopes in the curve for the grain can clearly be seen. The values of E_a for the grain in low and high (from where the effect of grain boundary starts) temperature regions were estimated, respectively, to be 0.76 eV and 0.27 eV. Also, the value of E_a for grain boundary was found to be 1.51 eV. The inset 1 of Fig. 11 shows the variation of ac conductivity with temperature at different frequencies. The value activation energy (= 0.84 eV at 100 Hz and 0.58 eV at 100 kHz) was obtained by least squares fitting of the data at higher temperature region. It is observed that the value of activation energy decreases with the increase in frequency. It can be seen that the ac conductivity is almost insensitive in the low temperature region irrespective of the operating frequencies. Also, the onset temperature (insensitive to sensitive region) shifts to the higher temperature side with an increment in frequency. The low value of activation energy obtained could be attributed to the influence of the electronic contribution to the conductivity. The increase in conductivity with temperature may be considered on the basis of that within the bulk, the oxygen vacancies due to the loss of oxygen are usually created during sintering and the charge compensation follows the reaction [28]: $O_o \rightarrow \frac{1}{2}O_2 \uparrow + V_o^{\bullet\bullet} + 2e^-$, which may leave behind free electrons making them n-type [29]. The low value of activation energy may be due to the carrier transport through hopping between localized states in a disordered manner. The minimum hopping length, R_{min} was estimated using the relation [30]:

$$R_{min} = 2e^2/\pi\varepsilon\varepsilon_o W_m \,. \tag{16}$$

The values of R_{min} were found to be of the order of 10^{-10} m in low, (room temperature to 300 °C) and 10^{-11} m in high (300 °C onwards) temperature regions. Also, the minimum hopping distance was found to be 10^{-4} times smaller than that of grain size in NST. The thermal conductivity data of grain and grain boundary for NST are shown in inset 2 of Fig. 11. NST showed a semiconductor like behaviour resulting in an increased electronic conduction of the total thermal conductivity. This electronic thermal conductivity account for the total thermal conductivity [31] and is given by:

$$\kappa = L\sigma T\left[1 + (3/4\pi^2)\{(E_a/k_B T) + 4\}^2\right], \tag{17}$$

where L is the Lorentz number. It is observed that the thermal conductivity of the grain as well as the grain boundary increases with increasing temperature and it exhibits reasonably low thermal conductivity.

4 Conclusions

Polycrystalline $(Na_{0.5}Sb_{0.5})TiO_3$, prepared through a high-temperature solid-state reaction technique, was found

to have a single-phase perovskite-type monoclinic structure. Impedance analysis indicated the presence of grain and grain boundary effects in NST. The dielectric relaxation in the system was found to be of the non-Debye type. The complex impedance plot and conductivity studies showed the NTCR character of NST. The correlated barrier hopping model was found to successfully explain the mechanism of charge transport in $(Na_{0.5}Sb_{0.5})TiO_3$.

REFERENCES

1 Y. Guo, K. Kakimoto, H. Ohsato, Solid State Commun. **129**, 279 (2004)
2 I.P. Raevski, S.A. Prosandeev, J. Phys. Chem. Solids **63**, 1939 (2002)
3 J.K. Lee, K.S. Hong, C.K. Kim, S.E. Park, J. Appl. Phys. **91**, 4538 (2002)
4 A. Simon, J. Ravez, Solid State Sci. **5**, 1459 (2003)
5 F. Bahri, H. Khemakhem, A. Simon, R. Von der Mühll, J. Ravez, Solid State Sci. **5**, 1235 (2003)
6 X.M. Chen, T. Wang, J. Li, Mater. Sci. Eng. B **113**, 117 (2004)
7 Y. Yuan, S. Zhang, C. Li, J. Mater. Sci. Mater. Electron. **15**, 601 (2004)
8 X.G. Tang, K.H. Chew, H.L.W. Chan, Acta Mater. **52**, 5177 (2004)
9 H. Abdelkefi, H. Khemakhem, G. Vélu, J.C. Carru, R. Von der Mühll, J. Alloys Compd. **399**, 1 (2005)
10 J.R. Gomah-Pettry, S. Saïd, P. Marchet, J.P. Mercurio, J. Eur. Ceram. Soc. **24**, 1165 (2004)
11 Q. Xu, S. Chen, W. Chen, S. Wu, J. Zhou, H. Sun, Y. Li, Mater. Chem. Phys. **90**, 111 (2005)
12 Y.M. Li, W. Chen, Q. Xu, J. Zhou, X. Gu, Mater. Lett. **59**, 1361 (2005)
13 Y.M. Li, W. Chen, J. Zhou, Q. Xu, X.Y. Gu, R.H. Liao, Physica B **365**, 76 (2005)
14 S.K. Barik, P.K. Mahapatra, R.N.P. Choudhary, Appl. Phys. A **85**, 199 (2006)
15 Lily, K. Kumari, K. Prasad, K.L. Yadav, J. Mater. Sci. (2006) in press
16 C.F. Buhrer, J. Chem. Phys. **36**, 798 (1962)
17 J. Suchanicz, K. Roleder, A. Kania, J. Handerek, Ferroelectrics **77**, 107 (1988)
18 K. Roleder, J. Suchanicz, A. Kania, Ferroelectrics **89**, 1 (1989)
19 Y. Hosono, K. Harada, Y. Yamashita, Japan. J. Appl. Phys. **40**, 5722 (2001)
20 J. Suchanicz, J. Kusz, H. Bhöm, H. Duda, J.P. Mercurio, K. Konieczny, J. Eur. Ceram. Soc. **23**, 1559 (2003)
21 C.K. Suman, K. Prasad, R.N.P. Choudhary, Adv. Appl. Ceram. **104**, 294 (2005)
22 J.R. Macdonald (Ed.), *Impedance Spectroscopy Emphasizing Solid Materials and Systems* (Wiley, New York, 1987)
23 P. Bonneau, O. Garnier, G. Calvarin, E. Husson, J.R. Gavarri, A.W. Hewat, A. Morrel, J. Solid State Chem. **91**, 350 (1991)
24 K. Funke, Prog. Solid State Chem. **22**, 111 (1993)
25 S.R. Elliott, Philos. Mag. B **37**, 553 (1978)
26 A.A.A. Youssef, Z. Naturforsch. **A57**, 263 (2002)
27 G.D. Sharma, M. Roy, M.S. Roy, Mater. Sci. Eng. B **104**, 15 (2003)
28 F.A. Kröger, H.J. Vink, Solid State Phys. **3**, 307 (1956)
29 K. Prasad, C.K. Suman, R.N.P. Choudhary, Ferroelectrics **324**, 89 (2005)
30 R. Salam, Phys. Stat. Solidi A **117**, 535 (1990)
31 E.A.E. Wahabb, Vacuum **57**, 339 (2000)